
ASSESSMENT OF DEEPONET FOR RELIABILITY ANALYSIS OF STOCHASTIC NONLINEAR DYNAMICAL SYSTEMS

A PREPRINT

Shailesh Garg

Department of Applied Mechanics
Indian Institute of Technology Delhi
Hauz Khas, New Delhi 110016, India.
shaileshgarg96@gmail.com

Harshit Gupta

Department of Mechanical Engineering
Indian Institute of Technology Delhi
Hauz Khas, New Delhi 110016, India.
harshit.gupta.iitd23@gmail.com

Souvik Chakraborty

Department of Applied Mechanics
School of Artificial Intelligence (ScAI)
Indian Institute of Technology Delhi
Hauz Khas, New Delhi 110016, India.
souvik@am.iitd.ac.in

February 1, 2022

ABSTRACT

Time dependent reliability analysis and uncertainty quantification of structural system subjected to stochastic forcing function is a challenging endeavour as it necessitates considerable computational time. We investigate the efficacy of recently proposed DeepONet in solving time dependent reliability analysis and uncertainty quantification of systems subjected to stochastic loading. Unlike conventional machine learning and deep learning algorithms, DeepONet learns is a operator network and learns a function to function mapping and hence, is ideally suited to propagate the uncertainty from the stochastic forcing function to the output responses. We use DeepONet to build a surrogate model for the dynamical system under consideration. Multiple case studies, involving both toy and benchmark problems, have been conducted to examine the efficacy of DeepONet in time dependent reliability analysis and uncertainty quantification of linear and nonlinear dynamical systems. Results obtained indicate that the DeepONet architecture is accurate as well as efficient. Moreover, DeepONet posses zero shot learning capabilities and hence, a trained model easily generalizes to unseen and new environment with no further training.

Keywords DeepONet · Neural Networks · Stochastic ODE · Nonlinear Systems

1 Introduction

While designing any engineering structure, performing appropriate tests to check the validity of the designs under various circumstances is of utmost importance. For a few cases where the forces acting on the system are predictable, analysis can be performed on a fixed set of samples to verify the design of the structure. However, in a majority of cases, the forces acting on the system are random in nature, and it is difficult for the designer to explicitly designate the design as pass or fail. For such cases, quantifying the uncertainties in the system, assessing its influence on system responses, and performing reliability analysis [1,2] becomes of utmost importance.

Reliability analysis is in a way a probabilistic study [3] of the system under consideration, and the ratio of favorable quantity to the total number of tests forms the basis of any probabilistic study. The same is reinforced in Bayesian statistics [4], which further states that uncertainties in the final results reduce when we have a sufficiently large number of samples. Thus to perform a robust reliability analysis in the face of uncertain forcing conditions, a large number of

input force realizations are generated, and a corresponding displacement ensemble is computed. We essentially test the system against a range of input forces to calculate its failure probability. To perform such a comprehensive analysis, both time and computational power are required, a shortage of which can lead to inadequate and unreliable design. Traditionally, system states for individual realizations of input force have been generated using integration schemes [5, 6] like Runge-Kutta Method [7] and Newmark Beta method [8, 9]. Techniques like Finite element modelling [10], MCMC simulation [11], importance sampling [12, 13] have also been used in the past. These schemes, however accurate, carry huge computational costs, thus limiting their use to a small number of test samples.

In order to reduce the computational requirements, one may choose to decrease the dimensionality of the data using techniques like Principal Component Analysis [14] or Independent Component Analysis [15], but however good the technique may be there is bound to be some information loss because of model order reduction [16]. To bypass these problems, one may use machine learning [17, 18] in conjunction with the traditional integration techniques. Machine learning is a budding field of research and has found its use across several industries [19–22]. Machine learning techniques, especially neural networks [23, 24] (NN) have the ability to learn from a small training data set and then apply that same knowledge to a vast data set with very little computational cost associated with it. Owing to this, several NN architectures have been developed with an aim to solve a set of differential equations or to learn nonlinear operators. Popular examples include Physics Informed NN [25], Fourier NN [26] and DeepONet [27].

In this paper, we propose using DeepONet, a neural network architecture, to prepare a surrogate model which can then be used to generate system states for multiple test samples with reduced computational cost. DeepONet was proposed by Lu Lu et al. in their paper [27], and it aims at learning the nonlinear operator based on a limited training data set. It is a data-driven architecture based on the universal approximation theorem [28] and can reliably solve ordinary differential equations and stochastic differential equations [29] (SDE). Results generated in this paper also indicate that given sufficient training data, DeepONet model demonstrates Zero-Shot Learning (ZSL) [30] capabilities for new inputs; this allows generalization of the proposed architecture.

The proposed surrogate model, while applicable for any dynamical system, is especially useful in cases where simulating high fidelity data is complex, and only a small set of the same can be generated. Results produced show that by only simulating a few hundred samples, thousands of samples can be inferred using the surrogate model with reasonable accuracy. It also gives the user ability to produce only relevant results i.e. if lets say displacements only at N^{th} DOF are required, traditional integration schemes require the displacements and velocities to be computed at all DOFs but using the trained surrogate model, user will be able to generate only the required data thus saving expensive server space. Additionally, for the cases where the simulation algorithm converges only for *fine* time steps, the proposed surrogate model can be trained at *coarser* time steps while retaining the integrity of the predictions, thus saving both computational cost and time. While other machine learning based surrogate algorithms are available in the literature which adopt Gaussian process or Kriging [31, 32], NNs [33] and other such techniques [34, 35], no work investigating the applicability of DeepONet for time-dependent reliability analysis and uncertainty quantification under forcing function uncertainty exists in the open literature, and owing to the benefits of DeepONet listed above, it is worthwhile to investigate its applicability on the same.

The remaining paper is arranged as follows, Section 2 discusses the problem statement of the paper while Section 3 introduces the DeepONet architecture being implemented. Section 4 showcases the various case studies carried out to test the proposed surrogate model. Finally, Section 5 draws the appropriate conclusion of the paper.

2 Problem Statement

Consider an N -DOF stochastic dynamical system with governing equation as follows:

$$\mathbf{M}\ddot{\mathbf{X}} + \mathbf{C}\dot{\mathbf{X}} + \mathbf{K}\mathbf{X} + \mathbf{N}(\mathbf{X}, \dot{\mathbf{X}}, \boldsymbol{\theta}_N) = \mathbf{F}, \quad (1)$$

where \mathbf{M} , \mathbf{C} and \mathbf{K} are the mass, damping and stiffness matrices respectively. $\mathbf{N}(\cdot)$ is the restoring force which is a nonlinear function of system states \mathbf{X} and parameter $\boldsymbol{\theta}_N$. $\mathbf{F} \sim \mathbb{P}(\cdot)$ is the input force vector drawn from the probability distribution $\mathbb{P}(\cdot)$. This uncertainty in the input force of Eq. (1) lends it its stochastic nature, thus necessitating reliability analysis.

Now, reliability analysis can be performed using various different techniques [36], choice of which depends on the need of the specific application. The first step, however is usually to draw realizations of input force from the respective probability distribution and solve Eq. (1) to generate a displacement ensemble. At which point, the methodologies diverge depending on the quantity being measured. In this paper, we will be computing First Passage Failure Time [37] (FPFT), which gives a Probability Density Function (PDF) for the failure time of the structure. Steps involved include taking realizations of displacement ensemble one by one and comparing them with the predetermined threshold. The time step at which each sample crosses the threshold first is noted, and for samples that never cross the time step the

final time is noted. PDFs for the resulting failure time vector are computed, and further design related decisions can then be made. The thresholds in a practical scenario are computed based on the design codes being followed and the type of structure being designed. A schematic of the steps involved in FPFT reliability analysis is shown in Fig. 1. As discussed earlier, the goal of this paper is to prepare a surrogate model of the Eq. (1), which can expeditiously

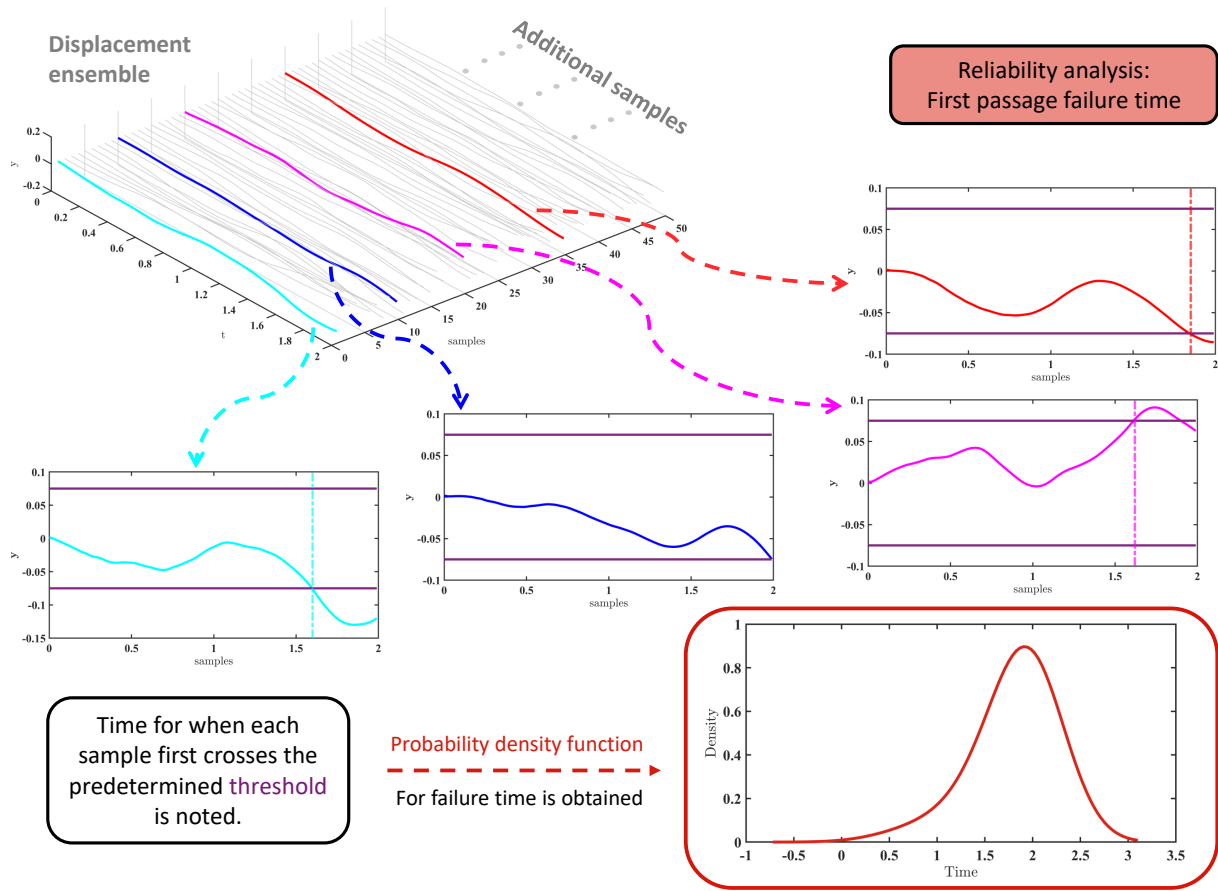


Figure 1: Pictorial representation of steps involved in reliability analysis. Specifically *first passage failure time* is computed. A displacement ensemble is generated using realizations of random input force. Each sample from the resulting ensemble is tested against a predetermined threshold, and the first time the threshold is crossed is noted for each sample. If the threshold is not crossed, the final time for that sample is recorded. The probability density function for the resulting time vector is obtained, and thus the probability of failure of the structure at any given time can be obtained.

generate results for a wide range of input forces. This will enable us to perform reliability analysis in a short amount of time, giving a thorough picture of the expected system behavior under various loading conditions. Steps involved in the proposed framework are given in Algorithm 1. A detailed schematic describing the process followed is shown

Algorithm 1: Proposed Framework

- 1 Identify governing equations and PDFs of the input forces for the system under consideration.
 - 2 Generate an ensemble of input forces and simulate training data using traditional integration schemes.
 - 3 Train the DeepONet model using the simulated training data.; ▷ Refer section 3.
 - 4 Predict displacement ensemble for new realizations of input force using the trained model.
 - 5 Perform reliability analysis on the system under consideration using the predicted displacement ensemble.
-

in Fig. 2. To prepare the aforementioned surrogate model, DeepONet architecture for learning nonlinear operators has been implemented. The neural network architecture is discussed in detail in the following section.

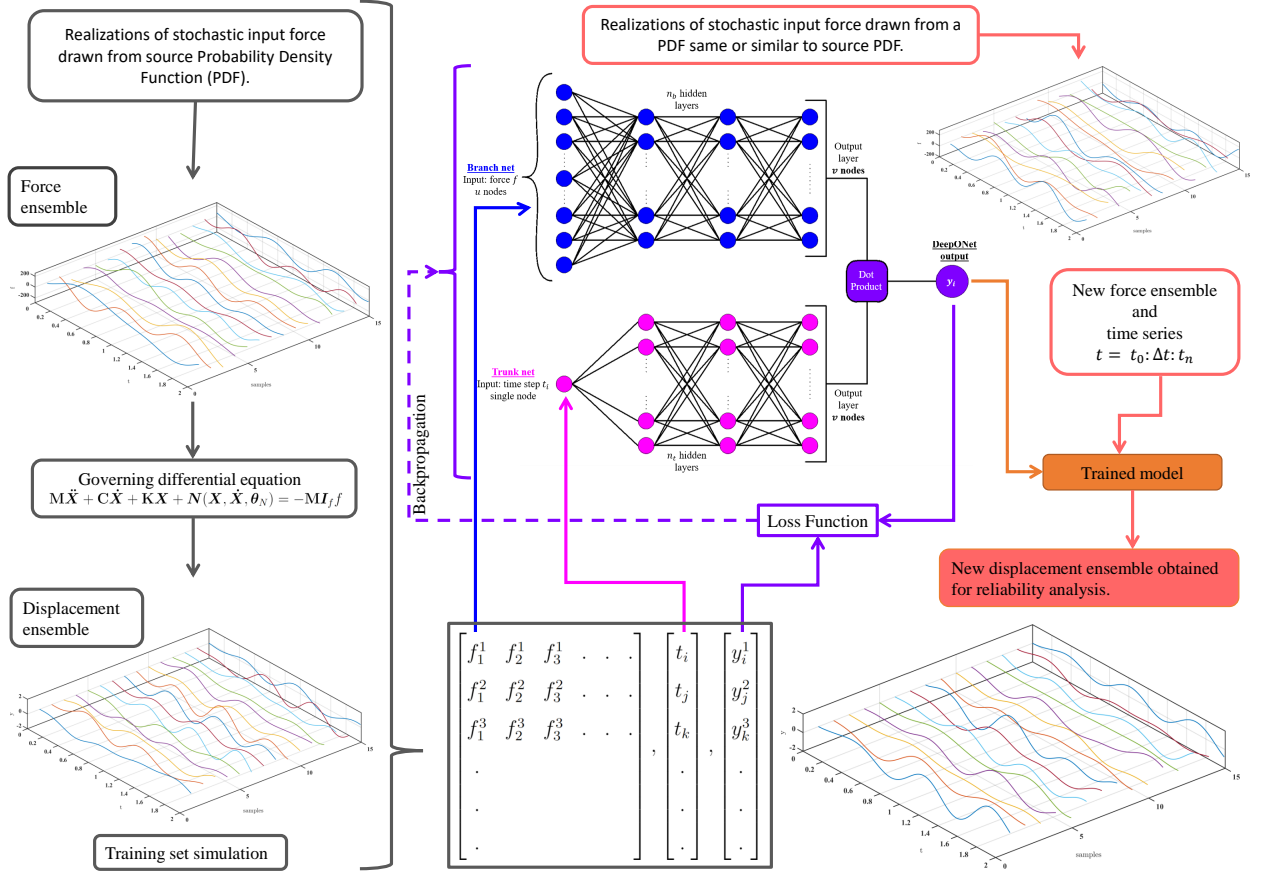


Figure 2: Schematic showcasing the process flow adopted in this paper. From a source PDF, realizations of input forces are generated, and based on the governing differential equation; displacement ensemble is obtained. The training data thus generated is rearranged as shown in Eq. (3) and is passed through the DeepONet architecture. The trained model obtained from DeepONet is then introduced to new realizations of input force, and the corresponding displacements are generated with reduced computational cost. These displacements are then used to perform reliability analysis on the system under consideration.

3 DeepONet

DeepONet is a neural network architecture developed to learn nonlinear continuous operators such as integrals, ODEs and stochastic ODEs. It is based on the universal approximation theorem, which states that even a single layer neural network is sufficient to learn a continuous nonlinear operator. In order to reduce the generalization error, DeepONet uses a branch and trunk architecture. The branch network is trained to encode the input function of the nonlinear operator while the trunk network encodes the domain of the input function. The two layers are then merged, and an output is generated. Schematic for DeepONet architecture is shown in Fig. 3, mathematical representation of the same is as follows:

$$G(f)(y) = \left\langle \alpha_b \left(b_b + \sum_i x_i^b w_i^b \right), \alpha_t \left(b_t + \sum_i x_i^t w_i^t \right) \right\rangle, \quad (2)$$

where $G(f)(y)$ is the target nonlinear operator with input f and output y . The quantities $\alpha_b \left(b_b + \sum_i x_i^b w_i^b \right)$ and $\alpha_t \left(b_t + \sum_i x_i^t w_i^t \right)$ are the outputs of branch and trunk network respectively. α_b and α_t in Eq.(2) represent the activation functions for the branch and trunk networks and, b_b and b_t are their respective bias. x^b and x^t are neurons corresponding to last layer of branch and trunk network having weights w^b and w^t respectively. $\langle \cdot, \cdot \rangle$ represents the dot product. Branch and trunk networks can also be configured in such a way that individually they are stacked

neural networks i.e. each neuron in unstacked DeepONet will be replaced by a neural network. In this paper, we use

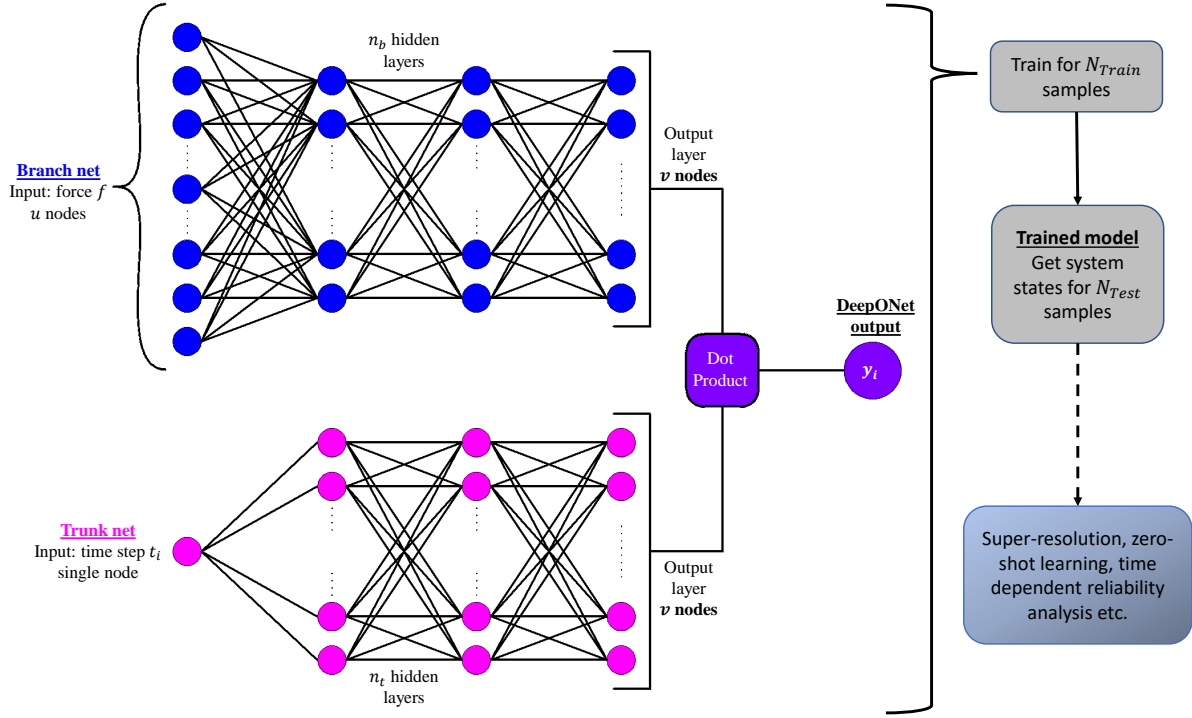


Figure 3: Flow chart showcasing the DeepONet architecture and how it has been used in the paper. DeepONet’s architecture is divided into two main parts namely branch net and trunk net. The branch net takes force f as input while the trunk net takes a random time step t_i as input. Respective inputs are then passed through branch net and trunk net, both having *same output size*. The corresponding outputs obtained are then combined and the final output in the form of displacement y_i corresponding to input time step t_i is obtained. Note, a normalization layer has been added in both branch and trunk net after the initial input layers.

unstacked DeepONet architecture which takes forcing function as input for branch network and random time step as input for the trunk network. Subsequently the output is the displacement corresponding to the input time step and the forcing function. The training data set for the used DeepONet architecture looks as follows:

$$\begin{bmatrix} f_1^1 & f_2^1 & f_3^1 & \cdot & \cdot & \cdot \\ f_1^2 & f_2^2 & f_3^2 & \cdot & \cdot & \cdot \\ f_1^3 & f_2^3 & f_3^3 & \cdot & \cdot & \cdot \\ \cdot & \cdot & \cdot & \cdot & \cdot & \cdot \\ \cdot & \cdot & \cdot & \cdot & \cdot & \cdot \end{bmatrix}, \begin{bmatrix} t_i \\ t_j \\ t_k \\ \cdot \\ \cdot \end{bmatrix}, \begin{bmatrix} y_i^1 \\ y_j^2 \\ y_k^3 \\ \cdot \\ \cdot \end{bmatrix}, \quad (3)$$

where $t_i \sim \mathbb{U}(0, t_{end})$ and y_i is the corresponding displacement. Characters in the superscript of f and y represent the sample numbers while in the subscript represent the time step. The loss function for the network is taken as the mean squared error ϵ function which is defined as follows:

$$\epsilon = \frac{1}{N_p} \sum_{i=1}^{N_p} (y_a - y_p)^2, \quad (4)$$

where y_a is the target output of $G(f)(y)$ and y_p is the output obtained from the neural network. N_p is the number of points and is equivalent to batch size in NN training. Algorithm 2 includes the steps involved in training the surrogate model. We have implemented the DeepONet architecture using Google’s Tensorflow [38] machine learning package.

4 Numerical Illustration

This section covers four different case studies exploring a variety of dynamical systems. Case-I covers a single Degree of Freedom (DOF) Bouc Wen system [39, 40] while Case-II deals with a 5-DOF system installed with a duffing

Algorithm 2: DeepONet Algorithm

```

1 Prepare the input data set; ▷ Refer Eq. (3)
2 for  $i = 1$ : no. of iterations do
3   for  $j = 1$ : no. of training data batches do
4     Input one batch of training force into branch net.
5     Input corresponding batch of random time steps into trunk net.
6     Merge the outputs from branch and trunk net; ▷ Refer Eq. (2)
7     Compute training error; ▷ Refer Eq. (4)
8     Update weights and biases based on back-propagation with an aim to reduce the training error.
9   end
10 end

```

oscillator at first DOF. A 76-storey building is covered in Case-III, and the same system is modified to include a Bouc Wen oscillator at first DOF for Case-IV. Training data for the DeepONet in the following case studies is sampled at a sampling frequency of 100Hz for 2 seconds. Input force applied in Case I(a) and II to IV is generated as follows:

$$f = \sum_{i=1}^{n_s} a_{s_i} \sin(f_{s_i} t) + \sum_{i=1}^{n_c} a_{c_i} \cos(f_{c_i} t), \quad (5)$$

where a_s and a_c are the amplitudes for sine and cosine wave respectively. f_s and f_c are frequencies for sine and cosine wave respectively. a_s, a_c, f_s and f_c are uniform random variables where $f_s, f_c \sim \mathbb{U}(0, 10)$ for all the case studies. $a_s, a_c \sim \mathbb{U}(-50, 50)$ for the first case study, $a_s, a_c \sim \mathbb{U}(-10, 10)$ for the second case study and $a_s, a_c \sim \mathbb{U}(-1, 1)$ for the third and fourth case study. n_s and n_c in Eq. (5) are the number of sine and cosine terms which together $n = n_s + n_c$ are referred to as Fourier terms (FT). Note, $n_s = n_c$ for even FT and $n_s = n_c + 1$ for odd number of FT. PDFs for the input force at a given time step, corresponding to different numbers of FT, is shown in Fig. 4. Fig. 5 shows the PDFs of different time samples in the displacement ensemble. Forcing function for Case I(b) is drawn

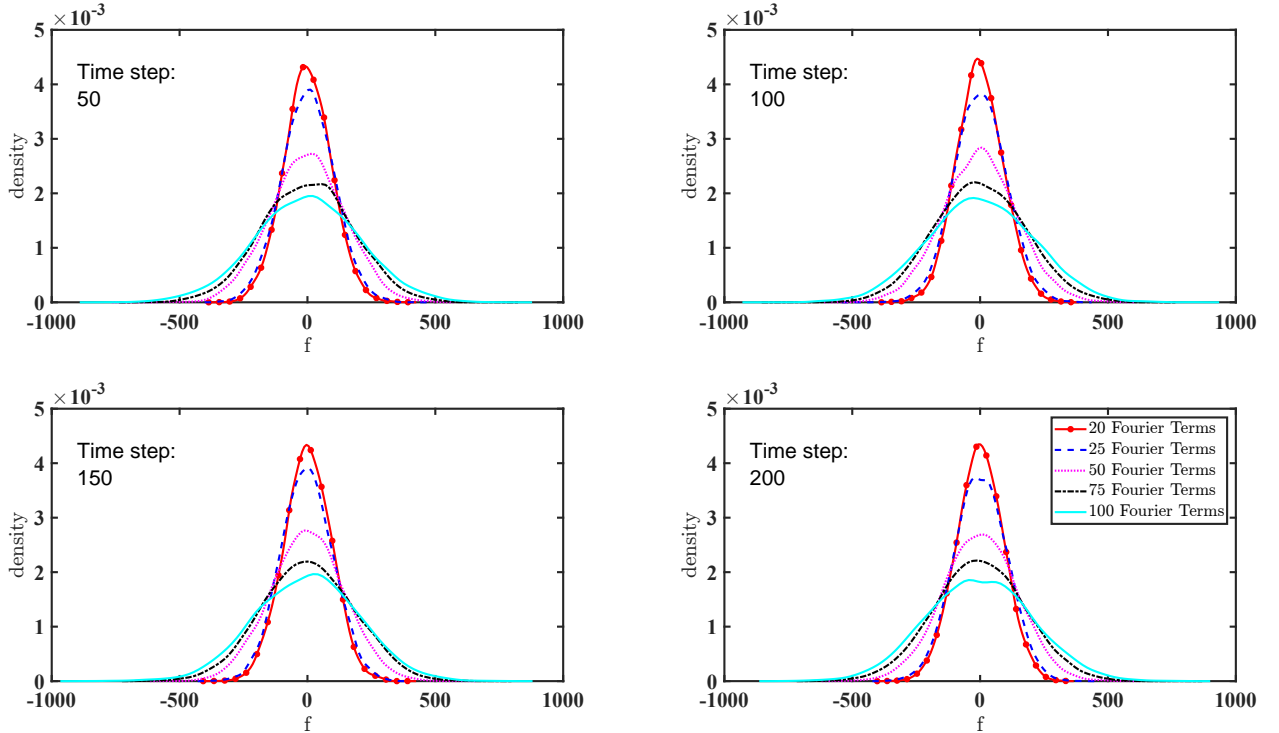


Figure 4: Probability density functions for input force computed at any particular time step. Comparisons have been drawn for cases where input force ensemble is generated using different number of FT.

from a Gaussian Process having squared exponential as its kernel function. Parameter details for the kernel and mean function are discussed in detail in the case study itself.

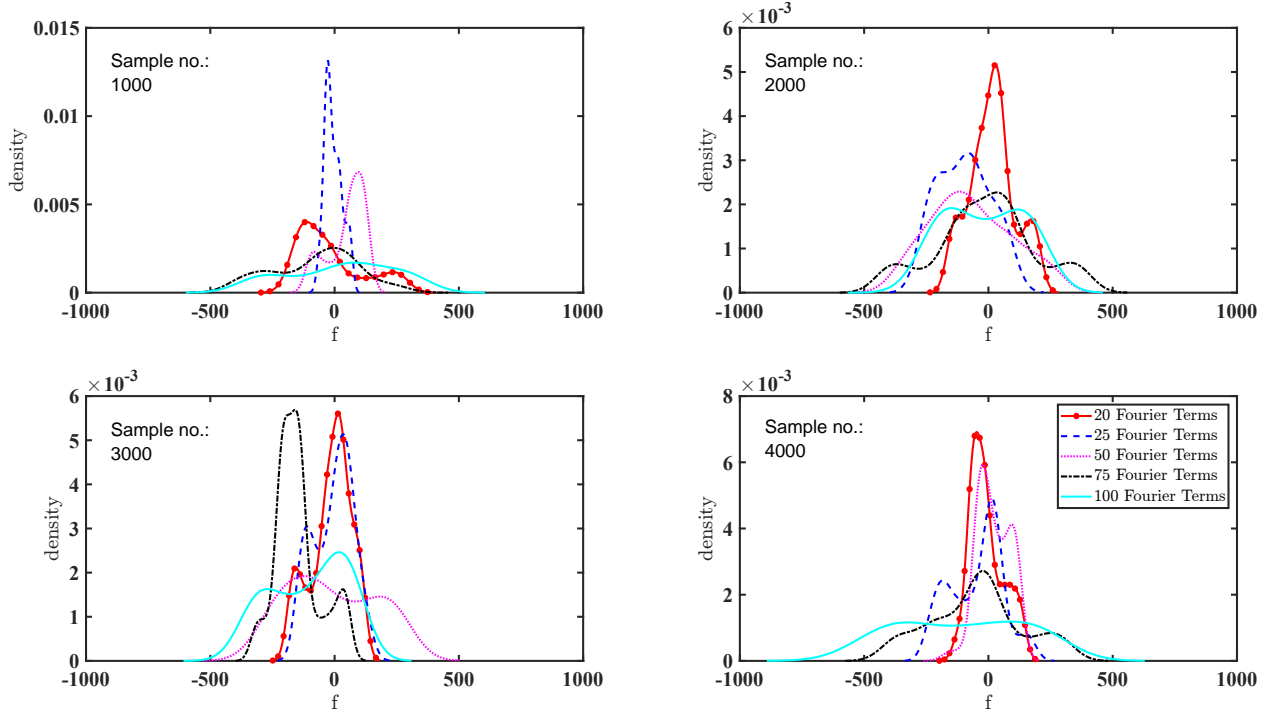


Figure 5: Probability density functions for individual samples of input force ensemble. Comparisons have been drawn for cases where input force ensemble is generated using different number of FT.

DeepONet architecture selected for the following case studies is as follows:

1. **Branch net:** 100 \rightarrow Batch Normalization \rightarrow 40 \rightarrow 40.
2. **Trunk net:** 1 \rightarrow Batch Normalization \rightarrow 40 \rightarrow 40.
3. **Output:** Dot product \rightarrow 1.

All layers except the final output layer with single node have ReLU activation function [41]. Glorot normal function [42] is used for initializing the weights. Unlike conventional ML algorithms, DeepONet generates function to function mapping (instead of variables to variables); this is why input for branch net is a realization of input force, which has been discretized into 100 points, thus necessitating 100 nodes in the input layer of branch net. The input size will change if forcing function is provided at finer or coarser intervals. The choice of number of hidden layer nodes is subjective and will change according to the needs of the application. For the following case studies however, nodes in hidden layers have been kept same.

4.1 Case-I: SDOF Bouc Wen System

For the first case study, the applicability of the surrogate model is tested for an SDOF Bouc Wen system. Governing equations for the system under consideration are as follows:

$$\begin{aligned} m\ddot{y} + c\dot{y} + ky + (1 - k_r)Q_y z &= f \\ \dot{z} &= \frac{1}{D_y}(\alpha\dot{y} - \gamma z|\dot{y}|z|^{n-1} - \beta\dot{y}|z|^n) \end{aligned} \quad (6)$$

where m , c and k are the mass, stiffness and damping matrices. Q_y , k_r , α , β , γ , D_y and η are the parameters of the Bouc Wen oscillator. Readers interested to read more about Bouc Wen oscillator may refer [39,40]. System parameters are selected from [43] and are given in Table 1.

4.1.1 Case-I (a)

Input forces for part *a* of Case-I have been generated using Eq. (5) with 20 FT. Testing and training data have been simulated based on Eq. (6) and initial conditions have been taken as $y_0 = 0.01$, $\dot{y}_0 = 0.05$. Comprehensive testing

Mass (Kg)	Stiffness (N/m)	Damping (Ns/m)	Nonlinear Parameters
$m = 6800$	$k = 232000$	$c = 3750$	$Q_y = 0.05mg, k_r = \frac{1}{6}, \alpha = 1,$ $\beta = 0.5, \gamma = 0.5, D_y = 0.0013, \eta = 2$

Table 1: System parameters for Case-I: SDOF Bouc Wen Oscillator.

has been carried out to test the surrogate model against a variety of setups and develop an intuition as to what works and why.

The Mean square error (MSE) values in Table 2 showcase the performance of surrogate model when trained for varying number of training samples. Initial samples vary from 25 to 150 with time steps per sample or points per sample (PPS) fixed at 100; implying that in case of 150 initial samples, displacements were simulated for 150 different input forces, and for each displacement 100 uniformly distributed time steps were serially selected for training. Once trained, displacement ensemble was generated using 10000 different input forces, and the DeepONet predictions were compared against the ground truth to get the MSE. It can be observed that as the number of initial samples increases, the MSE value decreases which is a direct effect of increased training data. In the same table, the performance of the trained model is also shown for cases where input forces are generated using different number of FT. As we increase the number of FT from 20 to 100 in prediction stage, the MSE values increase, but they are still negligible for the case with only 150 initial samples. This showcases ZSL capabilities of the surrogate model as it is able to produce good results for input distribution dissimilar to the one used for training.

M.S.E.		FT				
		20	25	50	75	100
Samples	25	5.54E-07	7.28E-07	2.25E-06	4.10E-06	6.09E-06
	50	7.33E-08	9.08E-08	2.58E-07	5.90E-07	1.03E-06
	75	7.86E-08	1.18E-07	5.02E-07	1.00E-06	1.61E-06
	100	7.11E-08	8.99E-08	2.67E-07	5.51E-07	9.01E-07
	150	9.50E-09	1.08E-08	2.77E-08	7.04E-08	1.48E-07

Table 2: MSE values comparing performance of surrogate model when trained for different number of initial samples, for Case-I (a). PPS are fixed at 100. Comparison is also drawn for case when tested for input corresponding to different number of FT. Note, that the training is done for 20 FT only.

Fig. 6 shows the results produced for sample number 1000 and Fig. 7 shows the ensemble mean, and variance of 10000 samples plotted against the ground truth when the model is trained using 150 initial samples having 100 PPS. The plots further validate the trend shown by the MSE values as the predicted values closely follow the ground truth.

Now that the variation in performance is tested for changing initial samples, another avenue of testing will be exploring the effects of changing PPS. Table 3 shows the MSE values for varying PPS, keeping the number of initial samples fixed at 150. It can be observed that as the number of PPS increases, the MSE value decreases. This is simply due to the fact that while training, if PPS are more, surrogate model will get a better representation of the output function, even when initial samples are kept same. Best performance among the tested PPS is observed for PPS equal to 100. It should be noted that in Tables 2 and 3 initial samples are as low as 50 with 100 PPS and PPS as low as 25 with initial samples as 150 show negligible MSE values. The choice of 150 initial samples with 100 PPS however gave the best results for ZSL. If the goal is only to perform predictions within the training distribution, fewer initial samples and/or PPS may also give good results.

M.S.E.		FT				
		20	25	50	75	100
PPS	1	6.11E-04	7.78E-04	1.69E-03	2.60E-03	3.47E-03
	25	9.16E-08	1.09E-07	2.65E-07	4.67E-07	8.72E-07
	50	2.46E-08	3.58E-08	1.65E-07	4.28E-07	8.18E-07
	75	1.53E-07	2.08E-07	6.86E-07	1.47E-06	2.52E-06
	100	1.66E-08	2.32E-08	1.09E-07	2.52E-07	4.92E-07

Table 3: MSE values comparing performance of surrogate model when trained for different number of PPS, for Case-I (a). Initial samples are fixed at 150. Comparison is also drawn for case when tested for input corresponding to different number of FT. Note, that the training is done for 20 FT only.

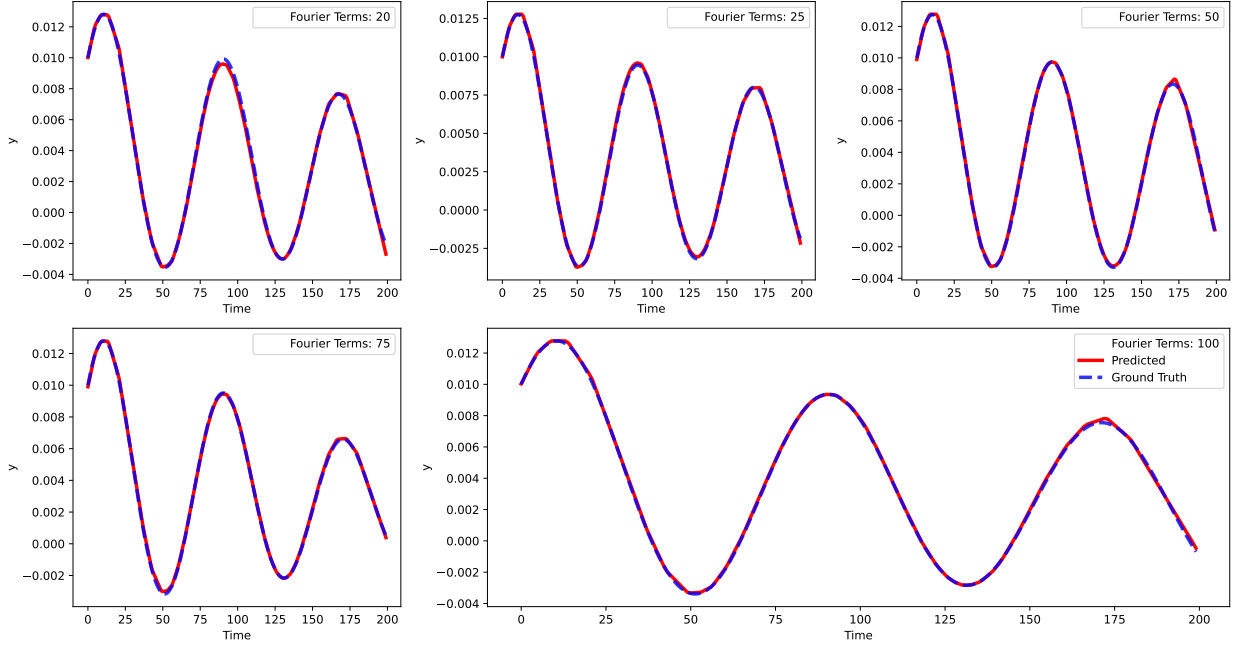


Figure 6: Predicted displacement for 1000^{th} sample compared against the ground truth, for Case-I (a). 150 initial samples are taken with 100PPS. Training is done for input forces corresponding to 20 FT.

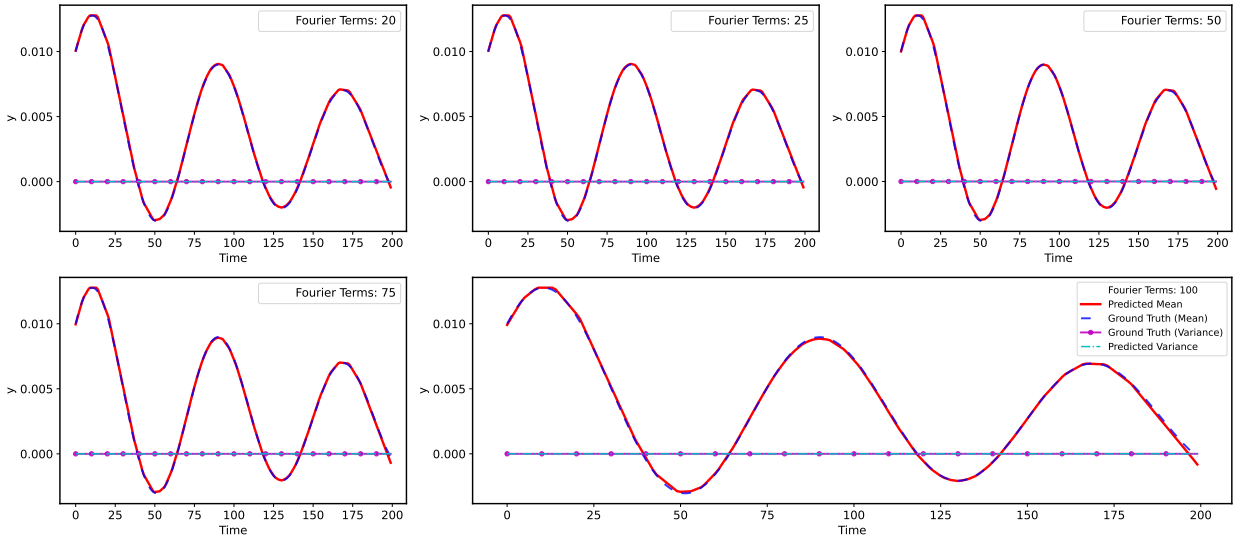


Figure 7: Predicted mean and variance of 10000 samples compared against the ground truth, for Case-I (a). 150 initial samples are taken with 100PPS. Training has been done for input forces corresponding to 20 FT.

4.1.2 Case-I (b)

For part *b*, input forces are taken as realizations of Gaussian process, which is defined as follows:

$$f \sim \mathcal{GP}(\mu(\boldsymbol{\theta}_\mu), \kappa(\boldsymbol{\theta}_\kappa)), \quad (7)$$

where $\mathcal{GP}(\cdot)$ is the Gaussian process with $\mu(\cdot)$ as its mean function and $\kappa(\cdot)$ as its kernel function. $\boldsymbol{\theta}_\mu$ and $\boldsymbol{\theta}_\kappa$ are the parameters for the mean and kernel function respectively. In this instance, f is taken as a zero mean Gaussian process

with squared exponential function as its kernel,

$$\kappa(t, t') = \sigma^2 \exp\left(-\frac{(t-t')^2}{2l^2}\right), \quad \theta_{\kappa} = [\sigma, l] \quad (8)$$

where σ is the variance parameter and l is the length scale parameter. Initial conditions for data simulation are taken as $y_0 = 0.005$ and $\dot{y}_0 = 0.001$. For training the surrogate model variance parameter is taken as $\sigma = 50$ and the length scale parameter is taken as $l = 0.10$. 1000 initial samples are taken for training the surrogate model with 50 PPS.

The surrogate model is tested for various combinations of σ and l and Fig. 8 shows the MSE of 10000 samples for each combination. It can be observed that while the MSE values are higher for length scale below 0.10, they are of the order 10^{-7} . Similarly, for values of σ more than 50, MSE values increase but stay within reasonable range. This shows the ZSL capabilities of the proposed framework. Equally good results were observed for 750 initial samples but are not included in the interest of avoiding recapitulation of similar results.

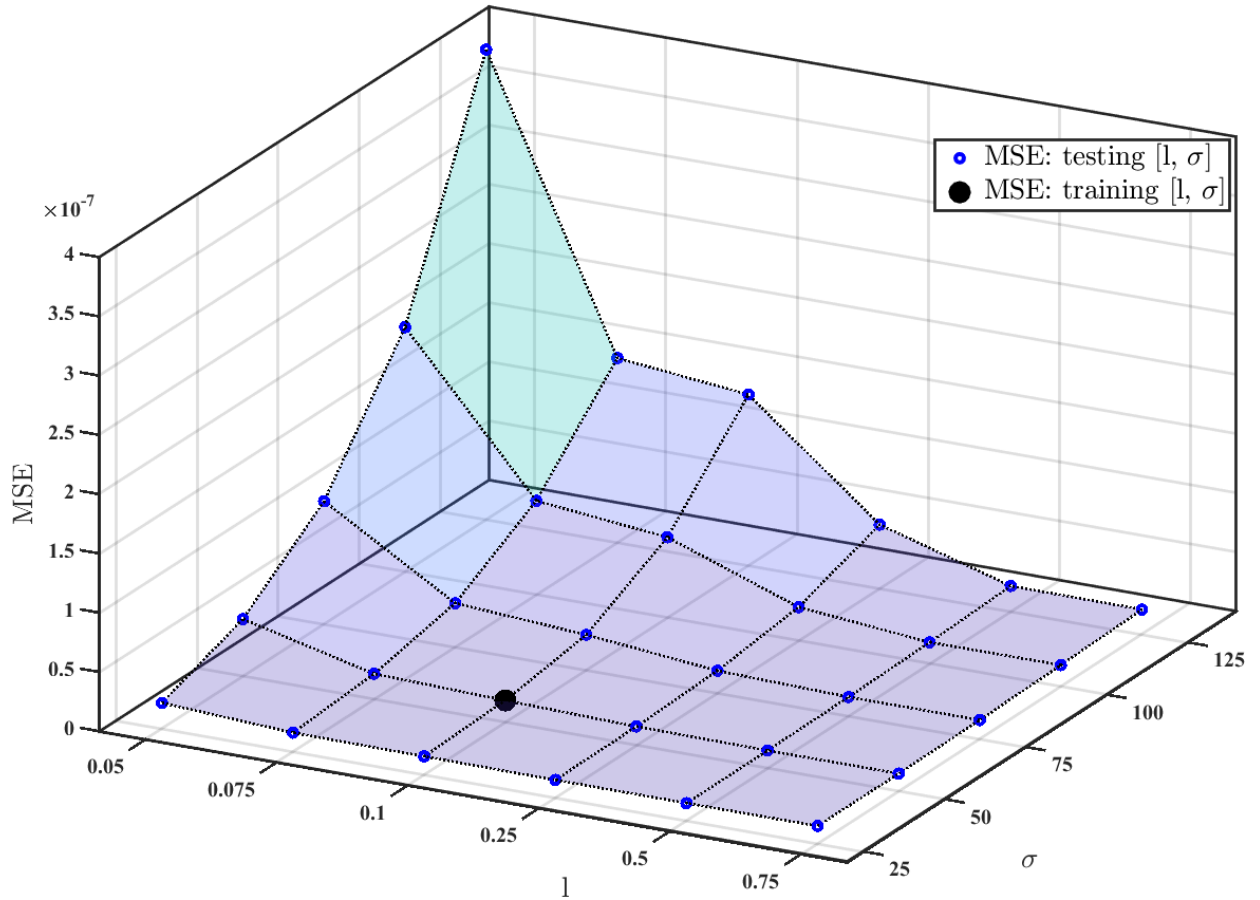


Figure 8: MSE values comparing performance of surrogate model when tested for different combinations of σ and l , for Case-I (b). Initial samples are fixed at 1000 with 50 PPS. Note, that the training is done for $\sigma = 50$ and $l = 0.10$

Fig. 9 shows the predicted mean and variance for 10000 test samples compared against the ground truth. As a detailed visual confirmation for the MSE values plotted earlier, comparisons have been drawn for four different combinations of σ and l , and as expected, predictions closely follow the ground truth.

In this case study, the behavior of the dynamical system was dominated by the initial conditions selected and the parameters of the nonlinear oscillator, but in the subsequent case studies, we will see the performance of the surrogate model for nonlinear multi DOF systems with non-zero initial conditions; whose behavior is rather significantly affected by the input force. Also, since the maximum displacement is observed at initial time steps only, reliability analysis is skipped for this system.

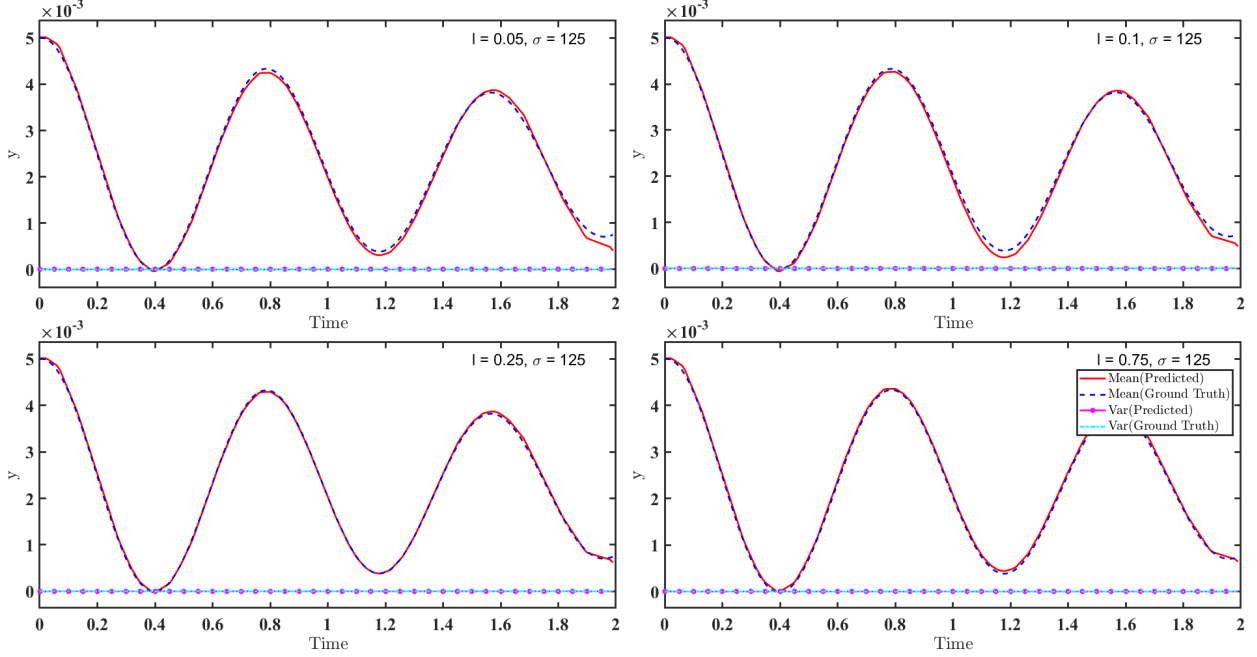


Figure 9: Predicted mean and variance of 10000 samples compared against the ground truth, for Case-I (b). 1000 initial samples are taken with 50PPS. Training is done for input forces corresponding to $\sigma = 50$ and $l = 0.10$.

4.2 Case-II: 5-DOF Nonlinear System

This case study deals with a base excited 5-DOF system with duffing oscillator installed at first DOF, governing equations of which are as follows:

$$\begin{aligned}
m_1\ddot{x}_1 + c_1\dot{x}_1 + c_2(\dot{x}_1 - \dot{x}_2) + k_1x_1 + k_2(x_1 - x_2) + \alpha_{do}x_1^3 &= -m_1f \\
m_2\ddot{x}_2 + c_2(\dot{x}_2 - \dot{x}_1) + c_3(\dot{x}_2 - \dot{x}_3) + k_2(\dot{x}_2 - \dot{x}_1) + k_3(\dot{x}_2 - \dot{x}_3) &= -m_2f \\
m_3\ddot{x}_3 + c_3(\dot{x}_3 - \dot{x}_2) + c_4(\dot{x}_3 - \dot{x}_4) + k_3(\dot{x}_3 - \dot{x}_2) + k_4(\dot{x}_3 - \dot{x}_4) &= -m_3f \\
m_4\ddot{x}_4 + c_4(\dot{x}_4 - \dot{x}_3) + c_5(\dot{x}_4 - \dot{x}_5) + k_4(\dot{x}_4 - \dot{x}_3) + k_5(\dot{x}_4 - \dot{x}_5) &= -m_4f \\
m_5\ddot{x}_5 + c_5(\dot{x}_5 - \dot{x}_4) + k_5(\dot{x}_5 - \dot{x}_4) &= -m_5f, \\
x_i(0) = 0.01, \dot{x}_i(0) = 0.05, i = [1, 2, 3, 4, 5] &
\end{aligned} \tag{9}$$

where m_i , c_i and k_i are the mass, damping and stiffness parameters respectively and α_{do} is the constant for duffing oscillator. f in this case study represents the ground acceleration, and randomness of input force is derived from the randomness of ground acceleration. Henceforth in Case-II to IV, ground acceleration and input force have been used interchangeably because in all three case studies, base excited systems have been considered. System parameters for the 5DOF system shown in Eq. (9) are given in Table 4. DeepONet architecture similar to previous case has been

Mass (Kg)	Stiffness (N/m)	Damping (Ns/m)	nonlinear Parameters
$m_1 = 10, m_2 = 10$ $m_3 = 9, m_4 = 9$ $m_5 = 7.5$	$k_1 = 10000, k_2 = 10000$ $k_3 = 9000, k_4 = 9000$ $k_5 = 7500$	$c_1 = 100, c_2 = 100$ $c_3 = 90, c_4 = 90$ $c_5 = 75$	$\alpha = 100$

Table 4: System parameters for Case-II: 5-DOF Duffing Oscillator.

adopted but for multi DOF systems, during training, f is mapped to displacements in parallel i.e. for this case study 5 trained models will be available at the end of analysis. PPS are taken equal to 25 and performance of surrogate model is tested for 500 and 1500 initial samples. Figs. 10 and 11 show the performance of surrogate model for different number of initial samples (500 and 1500 respectively) by comparing the mean and variance of the predicted displacements against the ground truth. 10000 test samples were considered while plotting each result. Predicted values closely follow the ground truth even for 500 samples and as expected, the results improve as the number of training samples increases.

To show the ZSL capabilities of the surrogate model, testing results for input force corresponding to 50FT are plotted in Fig. 12. The mean and variance of 10000 samples are shown, and good approximations of ground truth are obtained.

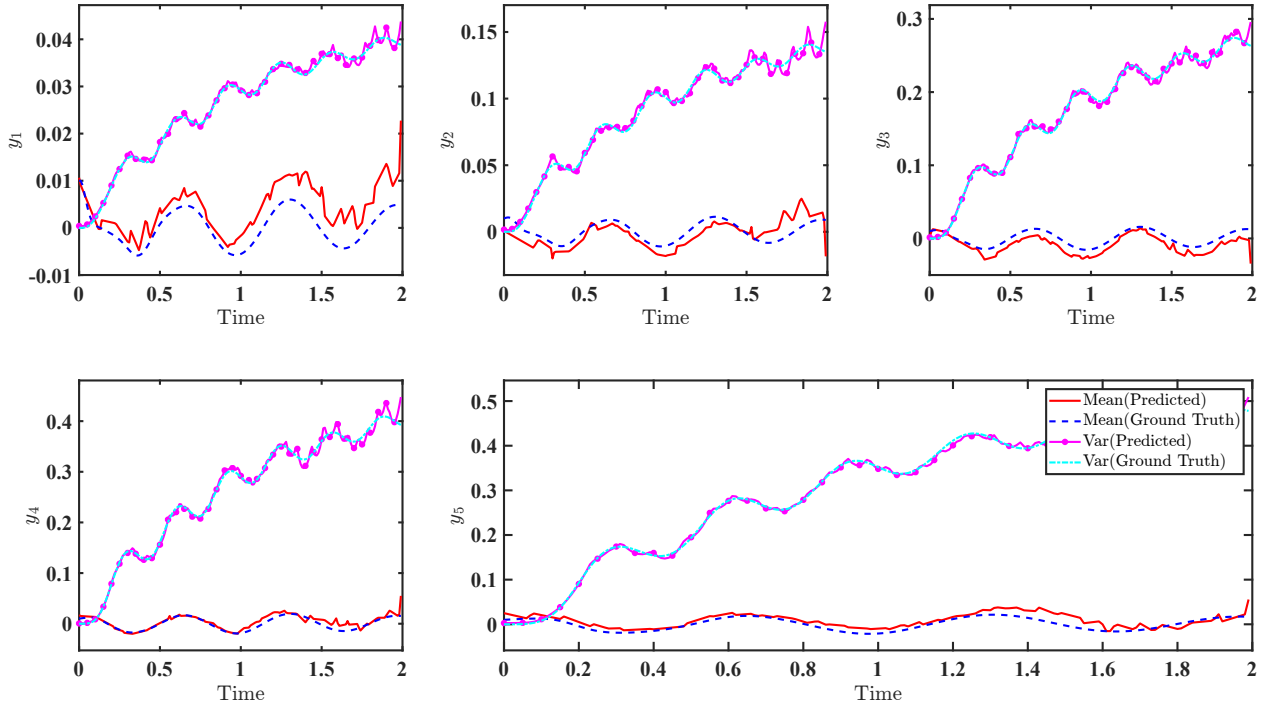


Figure 10: Predicted mean and variance of 10000 samples compared against the ground truth, for Case-II. 500 initial samples are taken with 25PPS. Training and testing has been done for input forces corresponding to 20 FT.

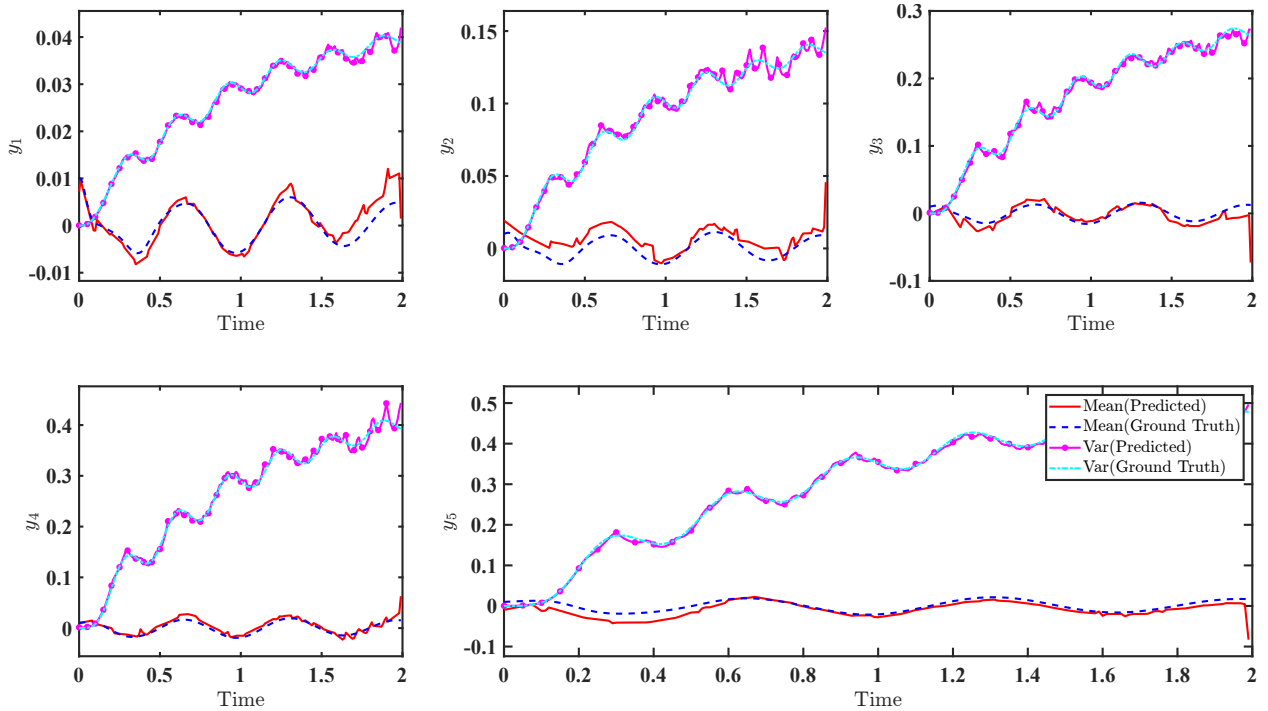


Figure 11: Predicted mean and variance of 10000 samples compared against the ground truth, for Case-II. 1500 initial samples are taken with 25PPS. Training and testing has been done for input forces corresponding to 20 FT.

It should be noted that the training here was done for input forces corresponding to 20 FT, with 1500 initial samples. To further support the mean and variance results, Fig. 13 shows the 5000th sample for case when the model is trained for 20 FT and predictions are made for 50 FT. From Fig. 13, it can be inferred that the minor gap observed in predicted

mean and ground truth in the Fig. 12 is trivial as compared to the actual magnitude of the displacement and thus has a negligible effect on the final predictions.

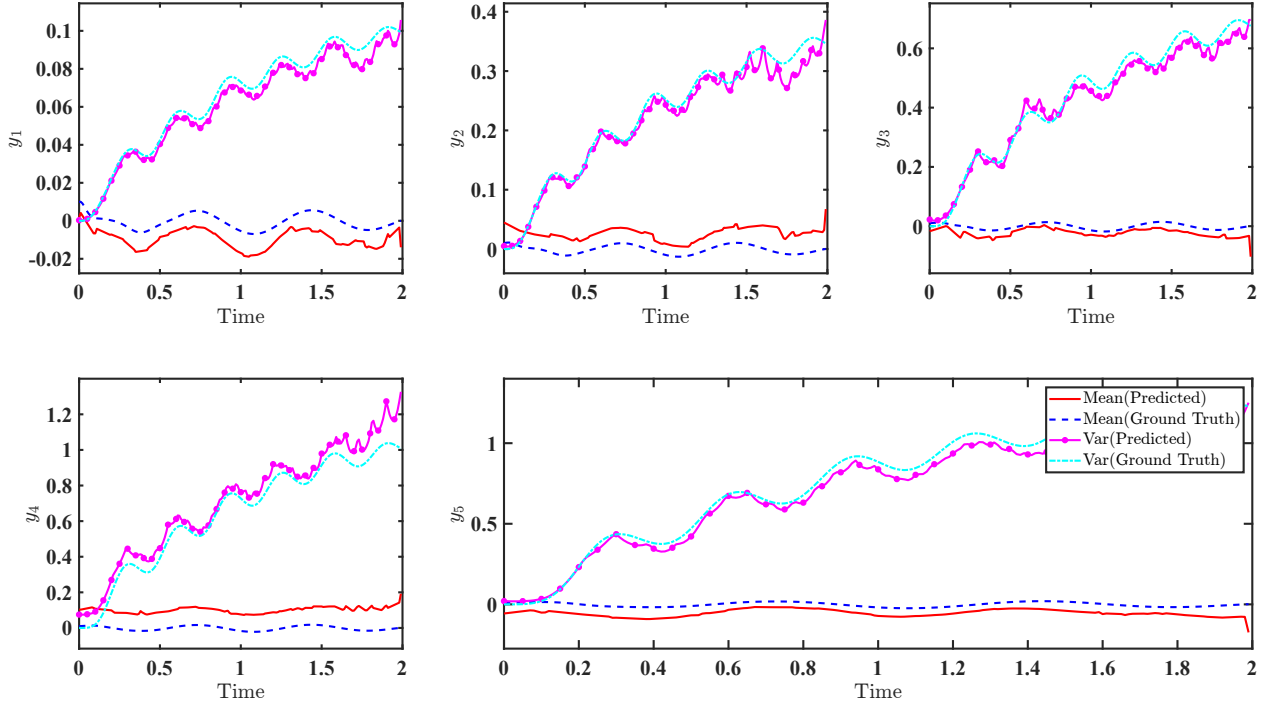


Figure 12: Predicted mean and variance of 10000 samples compared against the ground truth, for Case-II. 1500 initial samples are taken with 25PPS. Training is done for input forces corresponding to 20 FT and testing has been done for input forces corresponding to 50 FT.

Now that the predictions are available for a large number of testing samples, FPFT analysis can be performed. Fig. 14 shows the PDFs of FPFT for each DOF when the input force corresponds to 20FT. It can be observed that the predicted PDFs are similar to the actual PDFs, thus demonstrating the applicability of the surrogate model for reliability analysis. This case study is a perfect scenario where if the user wishes to obtain displacement at N^{th} -DOF, they can use the proposed surrogate model to obtain just that without producing the results for all the other DOFs, thus saving the computational time as well as expensive server space. This is possible because displacement at each DOF is trained and mapped to input force individually. The proposed surrogate model thus, in a sense, has the ability to decouple the N -DOF system without actually changing any of its dynamics or dropping any information. Another advantage of individually training the surrogate model is that if the MSE at any particular DOF is high, initial samples or PPS at that particular DOF only can be changed, thus optimizing the computational requirements at the training stage.

4.3 Case-III: 76-DOF ASCE Benchmark Building

This case study aims to showcase the scalability of the proposed approach by applying the concept of surrogate model to a base excited 76-DOF building, parameters for which are selected based on the ASCE benchmark [44, 45]. The differential equation for the system under consideration is as follows:

$$\mathbf{M}\ddot{\mathbf{X}} + \mathbf{C}\dot{\mathbf{X}} + \mathbf{K}\mathbf{X} = -\mathbf{M}\mathbf{I}_f f, \quad (10)$$

where \mathbf{I}_f is the influence vector, and f is the random ground acceleration, computed using Eq. (5). Initial displacements of 0.001 and initial velocities of 0.005 were also considered at all DOFs. Keeping DeepONet architecture same as that used in previous cases, initial samples for this case study are taken equal to 400 with 100 PPS each. Similar to the previous MDOF case, f will be mapped in parallel to displacements, and hence 76 different trained models will be available. This brings with it the advantage of training displacements at only required DOFs, thus saving computational cost and time. Fig. 15 shows the plot comparing mean and variance of predicted displacements against the ground truth at 10^{th} , 15^{th} , 35^{th} , 65^{th} and 75^{th} DOF when tested and trained for 20 FT and Fig. 16 shows the results for one particular sample (1000^{th} sample). Results show that the predicted values closely follow the ground truth, thus demonstrating the predictive capabilities of the proposed approach.

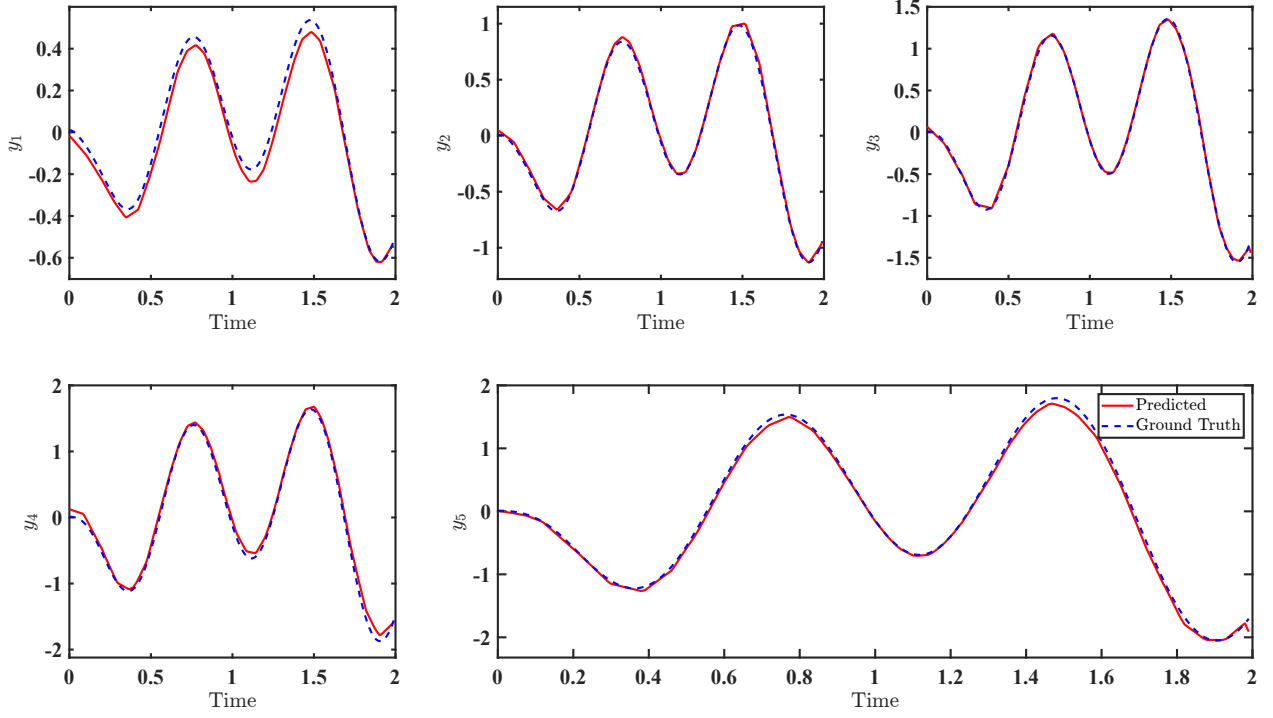


Figure 13: Predicted displacement for 5000th sample compared against the ground truth, for Case-II. 1500 initial samples are taken with 25PPS. Training is done for input forces corresponding to 20 FT and testing has been done for input forces corresponding to 50 FT.

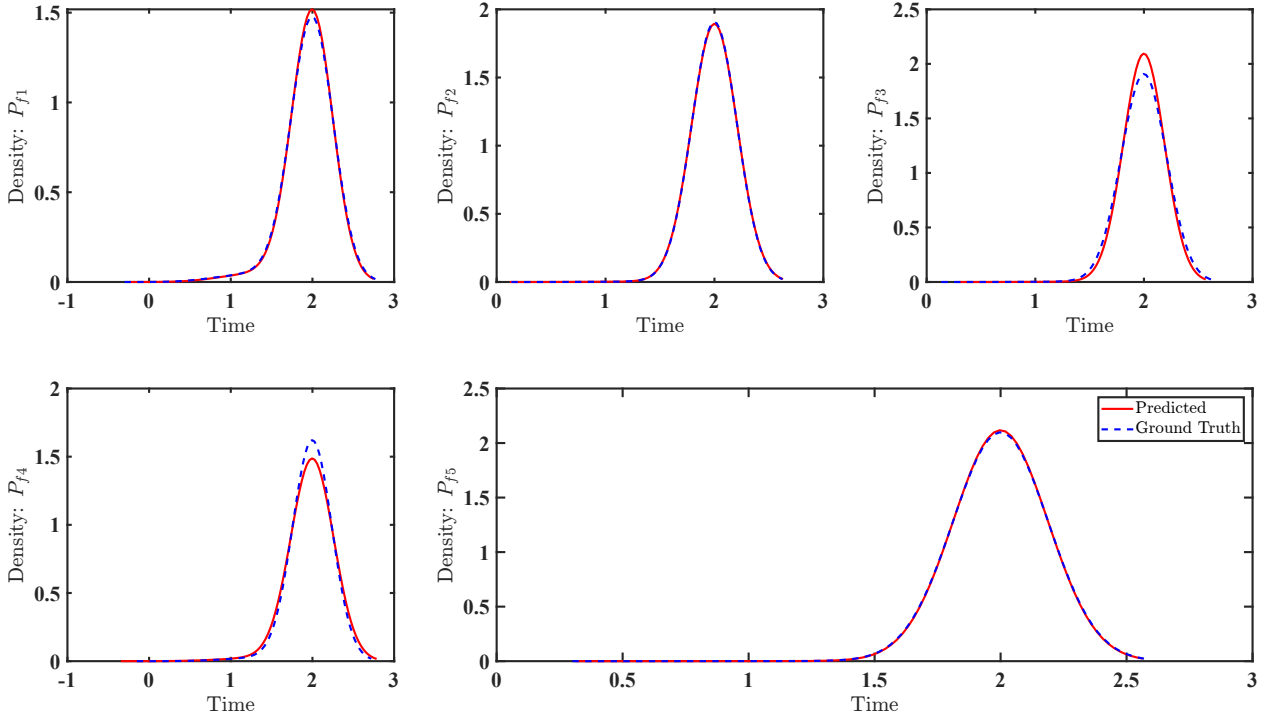


Figure 14: PDFs of FPFT obtained for Case-II. Training and testing are done for input forces corresponding to 20FT.

Fig. 17 shows the percentage normalized mean square error (NMSE) for case when surrogate model is trained for input forces corresponding to 20 FT and testing is carried out for 20 FT, 25 FT and 50 FT. The results produced show

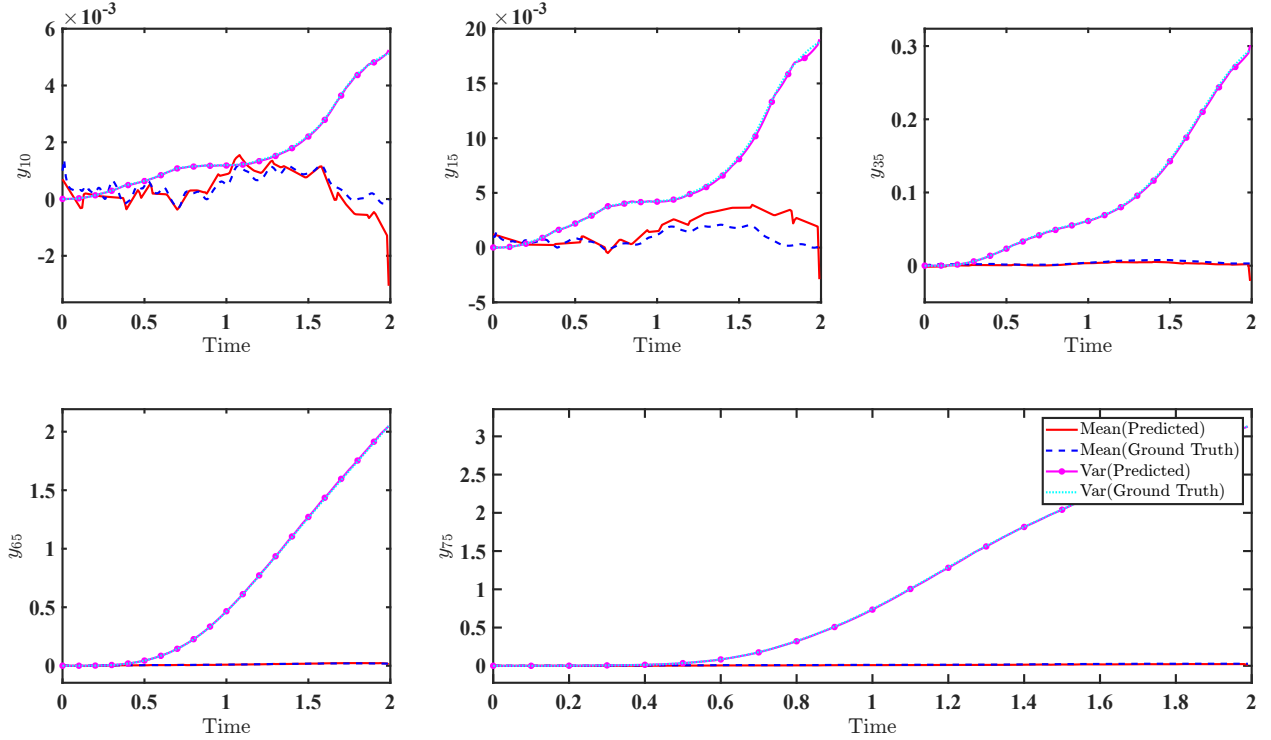


Figure 15: Predicted mean and variance of 10000 samples compared against the ground truth, for 76-DOF linear ASCE benchmark (Case-III). Results are shown at 10th, 15th, 35th, 65th and 75th DOF. Training and testing has been done for input forces corresponding to 20 FT.

the percentage NMSE error stays well within 5% for the majority of cases and well within 2% for 20 FT and 25 FT. NMSE has been calculated as follows:

$$NMSE = \frac{1}{N_s} \sum_{i=1}^{N_s} \frac{\|predicted - actual\|_2^2}{\|actual\|_2^2}, \quad (11)$$

where N_s is the number of samples.

Now, for reliability analysis, Fig. 18 shows the results for FPFT analysis at 10th, 15th, 35th, 65th and 75th DOF. The results closely follow the ground truth for the 76-DOF building, thus demonstrating the scalability of the proposed approach. Training and testing for the reliability analysis is done for input forces corresponding to 20FT.

4.4 Case-IV: 76-DOF nonlinear system

To further showcase the robustness and explore the advantages of the proposed surrogate model, 76-DOF building used in the previous case study is modified to include a Bouc Wen oscillator at first DOF. It is assumed that the nonlinear terms will prominently affect the differential equation at first DOF only, and appropriate changes have been made in the differential equations of the system. For data simulation using Runge-Kutta scheme, a sampling frequency of 12500Hz was adopted, but data provided for training was sampled at a frequency of 100Hz. The rest of the DeepONet architecture was kept similar to previous case studies, with initial samples here also being 400 with 100 PPS.

Fig. 19 shows the percentage NMSE for 10000 samples at each DOF. The results produced show that the NMSE is well below 1% thus giving a reasonably accurate picture of the actual system. To further showcase the performance of the surrogate model, Fig. 20 compares the predicted mean and variance with the ground truth. As expected, the model is able to predict with great accuracy, the displacements for the new input forces.

Similar to previous case studies, FPFT PDFs have been computed and are plotted in Fig. 21 for 5th, 15th, 35th, 65th and 75th DOF. The predicted PDFs closely follow the ground truth, thus enabling the designer to make well-informed decisions. Note, that the displacements produced for Case-III and Case-IV, 76-DOF buildings have high magnitudes

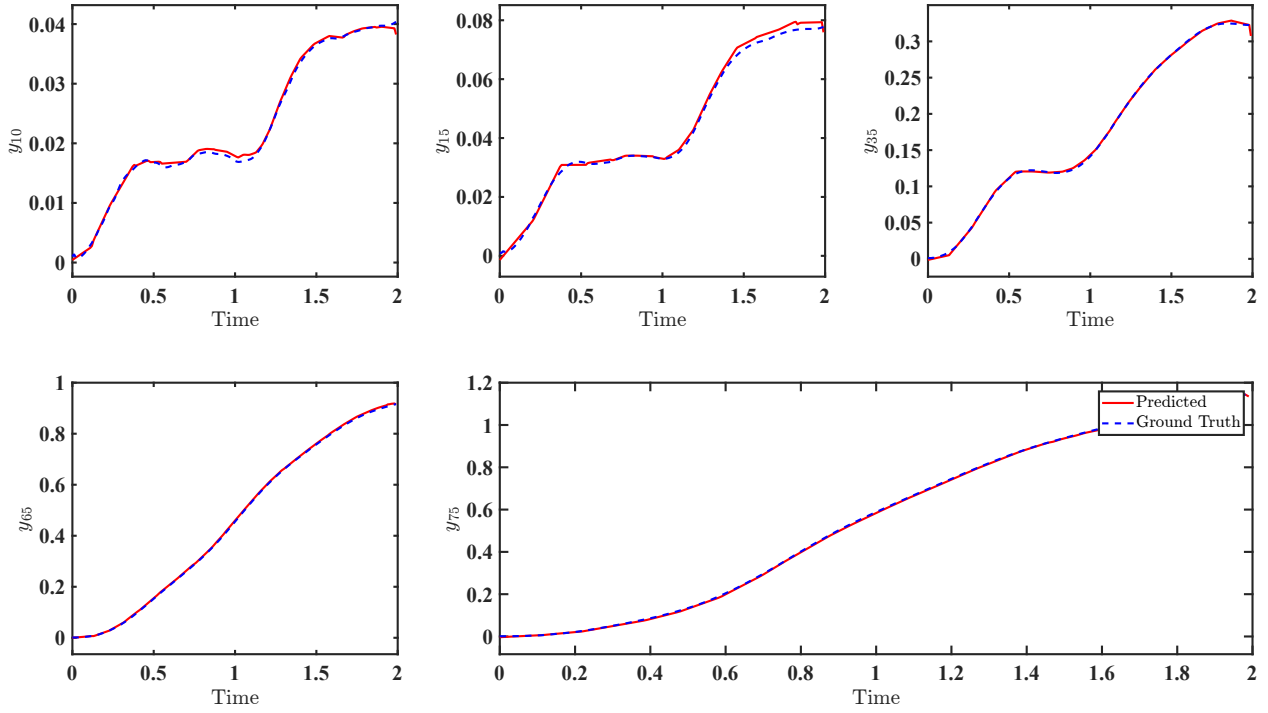


Figure 16: Predicted displacement for 1000th sample compared against the ground truth, for 76-DOF linear ASCE benchmark (Case-III). Results are shown at 10th, 15th, 35th, 65th and 75th DOF. Training and testing has been done for input force corresponding to 20 FT.

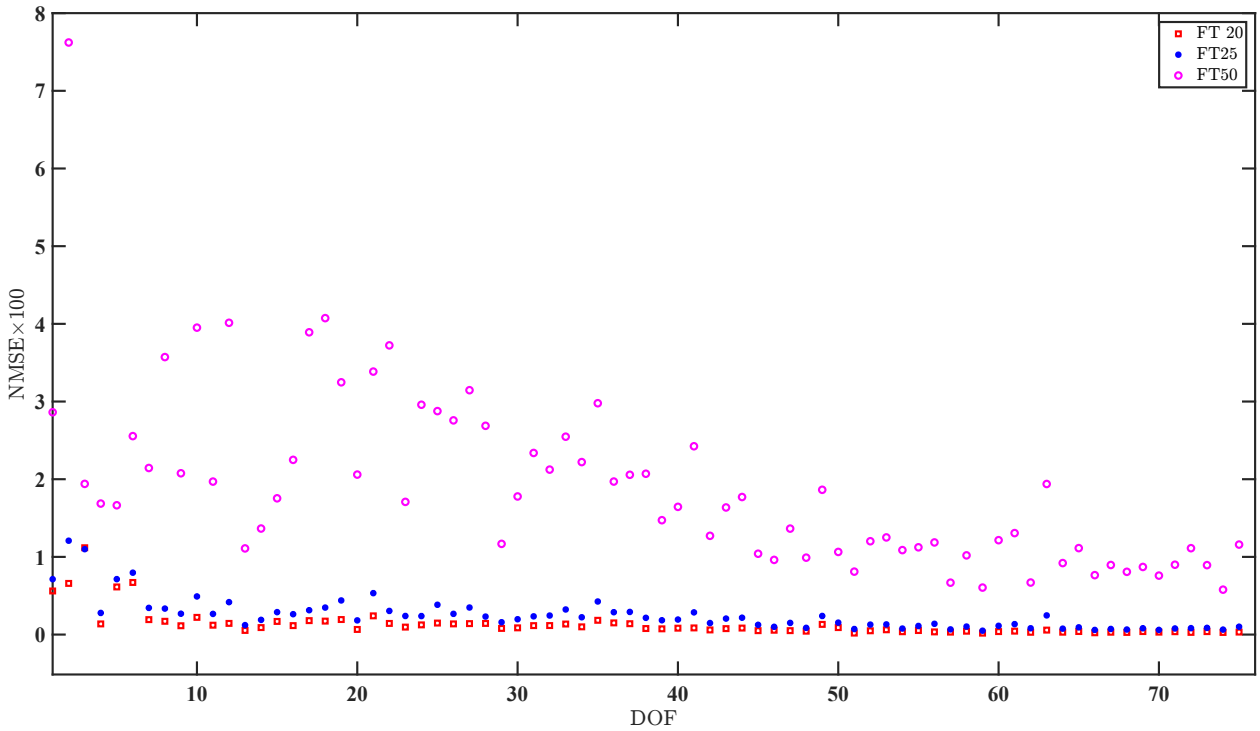


Figure 17: Percentage NMSE for 10000 samples. Model has been trained for input forces corresponding to 20 FT and testing has been done for 20 FT, 25 FT and 50 FT.

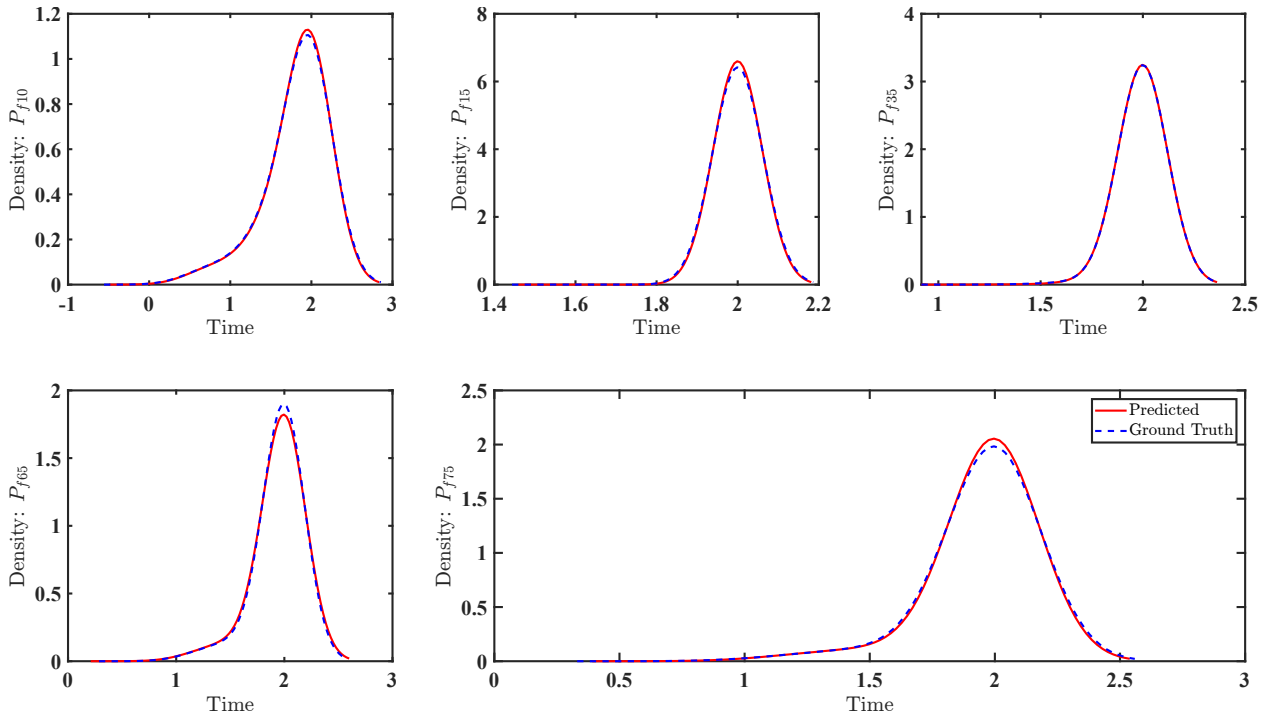


Figure 18: PDFs of FPFT obtained for Case-III at 10th, 15th, 35th, 65th and 75th DOF. Training and testing are done for input forces corresponding to 20FT.

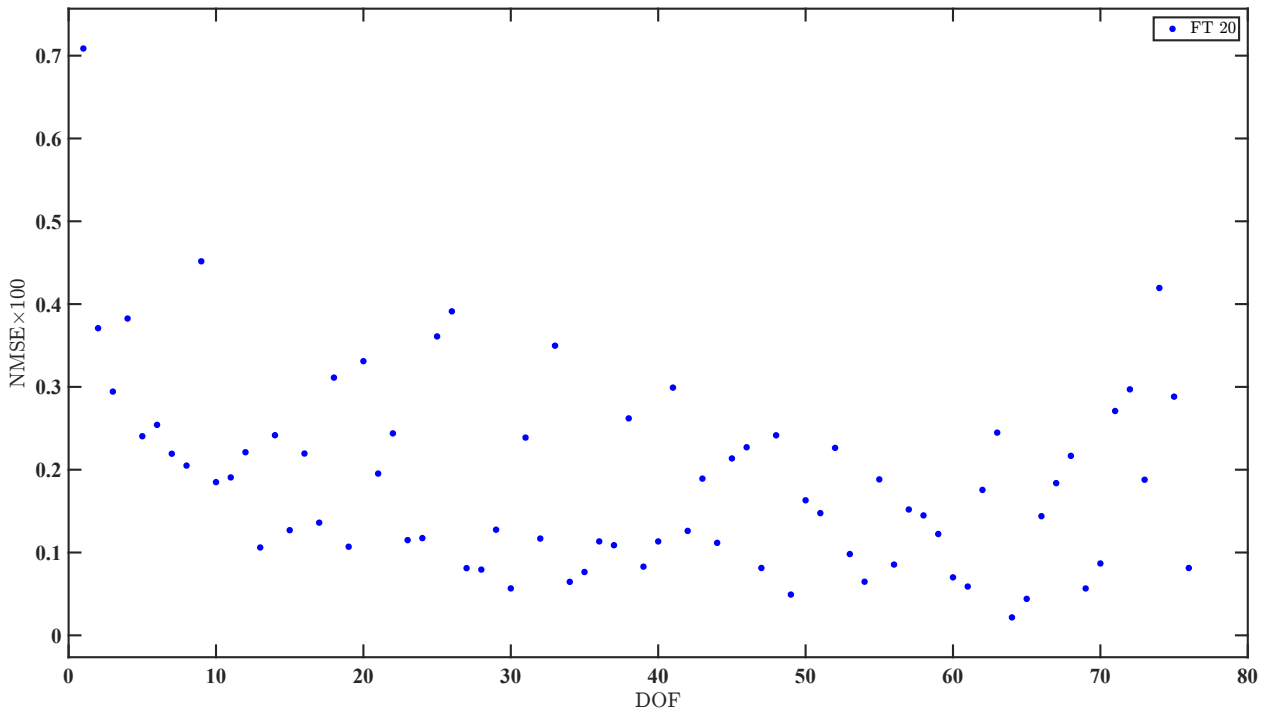


Figure 19: Percentage NMSE for 10000 samples (Case-IV). Model has been trained and tested for 20 FT.

for top stories as no control structure have been included in the analysis and despite this the surrogate model is still able to predict the displacements with great accuracy. The Python source code for the case studies discussed above are available at [link to be added here later](#).

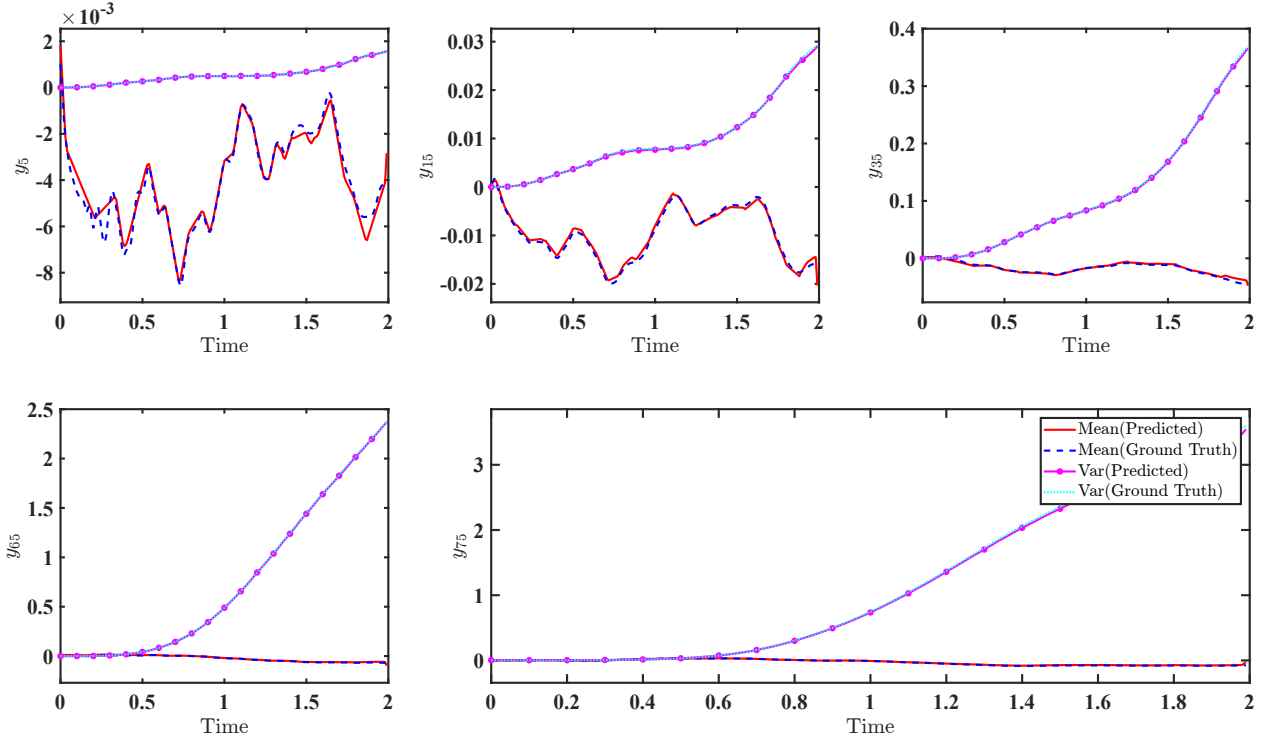


Figure 20: Predicted mean and variance of 10000 samples compared against the ground truth, for 76-DOF nonlinear building (Case-IV). Results are shown at 5^{th} , 15^{th} , 35^{th} , 65^{th} and 75^{th} DOF. Training and testing has been done for input forces corresponding to 20 FT.

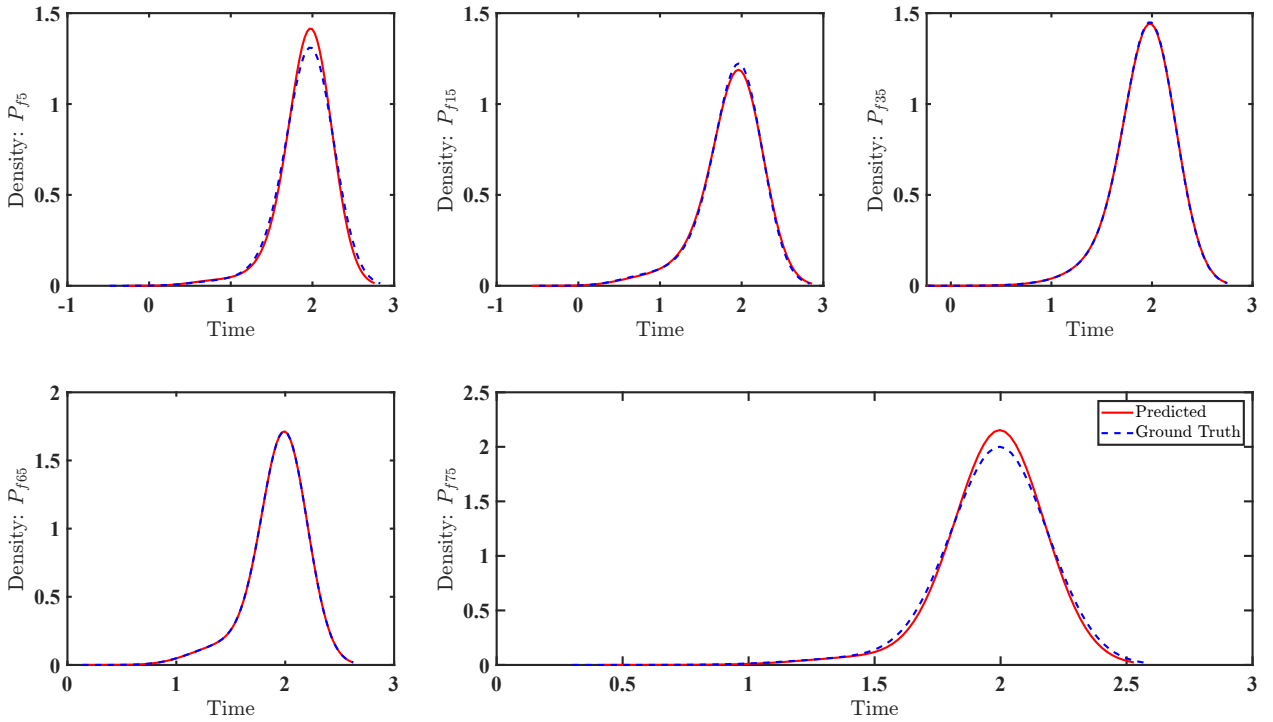


Figure 21: PDFs of FPFT obtained for Case-IV at 5^{th} , 15^{th} , 35^{th} , 65^{th} and 75^{th} DOF. Training and testing are done for input forces corresponding to 20FT.

5 Conclusion

Reliability analysis is an integral part of any structural design, especially for structures subjected to uncertain loading conditions, and to perform a robust reliability analysis, ample data representing the actual system is often needed. To achieve this, help of computer aided simulations is taken, as it is possible to test a wide variety of cases with little modification to underlying code. But generating high-fidelity data has associated with it immense computational cost, especially for complex nonlinear dynamical systems. In this paper, we propose a surrogate model based technique to perform reliability analysis using neural networks, specifically DeepONet architecture. Unlike conventional machine learning models, DeepONet learns a function to function mapping and hence, is ideally suited for time-dependent reliability analysis and uncertainty quantification problems subjected to loading uncertainty. The proposed framework enables efficient reliability analysis and uncertainty quantification subjected, and also provides ZSL capabilities. Using the proposed framework, it is possible to predict only the required data at coarser time steps, thus saving both expensive server space and computational cost. Authors note that time will be spent on training the surrogate model, but the time saved in the prediction stage will sufficiently compensate for the time spent in training. The proposed framework will especially benefit applications where the data simulation takes enormous amounts of time.

As a proof of concept, several case studies have been discussed above, testing the surrogate model against a variety of dynamical systems and assessing the use of DeepONet architecture for reliability analysis of nonlinear dynamical systems. Case-I and II demonstrate the surrogate model's capability to model nonlinear oscillators, while Case III and IV showcase the scalability of the proposed framework. Although at this stage, the predictions have been made for 10^4 samples, in a practical scenario, 10^5 or even more test samples may be required, and in those cases, the proposed algorithm can be immensely helpful in saving simulation time. The results produced in the case studies represent the actual system with good accuracy. Initial samples were kept limited so as to showcase the performance of surrogate model with less training data, and from the case studies, it can be observed that good results are obtained.

Based on the requirements of the system under consideration, DeepONet architecture can be easily tweaked, and appropriate results can be obtained. Some key points to note include the following. PPS selected should be uniformly distributed in the domain of the function for best training results. Number of nodes and hidden layers may be increased if the length of individual samples in the training data are large. As a rule of thumb, we recommend increasing the number of hidden layers first, before moving on to nodes per layer as this approach mitigates some chances of over-fitting. Apart from this, importance of normalization in any NN architecture can not be overstated, and hence the data being given as the training input should be appropriately normalized. Although the choice of normalization will depend on the application and type of data, we propose using Keras *preprocessing normalization layer* [46]. Min-max scaling function was also tested, and satisfactory results were obtained. Overall, it is safe to conclude that DeepONet does a decent job in time-dependent reliability analysis and uncertainty quantification subjected to stochastic loading.

Acknowledgment

SG acknowledges the support received from the Ministry of Education in the form of Ph.D. scholarship. SC acknowledges the financial support received from IIT Delhi.

References

- [1] Rüdiger Rackwitz. Reliability analysis—a review and some perspectives. *Structural safety*, 23(4):365–395, 2001.
- [2] Robert E Melchers and André T Beck. *Structural reliability analysis and prediction*. John Wiley & sons, 2018.
- [3] Jae-Ohk Lee, Young-Soon Yang, and Won-Sun Ruy. A comparative study on reliability-index and target-performance-based probabilistic structural design optimization. *Computers & structures*, 80(3-4):257–269, 2002.
- [4] William M Bolstad and James M Curran. *Introduction to Bayesian statistics*. John Wiley & Sons, 2016.
- [5] W Rüemelin. Numerical treatment of stochastic differential equations. *SIAM Journal on Numerical Analysis*, 19(3):604–613, 1982.
- [6] Keith W Morton and David Francis Mayers. *Numerical solution of partial differential equations: an introduction*. Cambridge university press, 2005.
- [7] John Charles Butcher. A history of runge-kutta methods. *Applied numerical mathematics*, 20(3):247–260, 1996.
- [8] K Subbaraj and MA Dokainish. A survey of direct time-integration methods in computational structural dynamics—ii. implicit methods. *Computers & structures*, 32(6):1387–1401, 1989.

- [9] Mario Paz. *Structural dynamics: theory and computation*. Springer Science & Business Media, 2012.
- [10] Barna Szabó and Ivo Babuška. *Finite element analysis*. John Wiley & Sons, 1991.
- [11] Reuven Y Rubinstein and Dirk P Kroese. *Simulation and the Monte Carlo method*, volume 10. John Wiley & Sons, 2016.
- [12] S Engelund and R Rackwitz. A benchmark study on importance sampling techniques in structural reliability. *Structural safety*, 12(4):255–276, 1993.
- [13] Iason Papaioannou, Costas Papadimitriou, and Daniel Straub. Sequential importance sampling for structural reliability analysis. *Structural safety*, 62:66–75, 2016.
- [14] Svante Wold, Kim Esbensen, and Paul Geladi. Principal component analysis. *Chemometrics and intelligent laboratory systems*, 2(1-3):37–52, 1987.
- [15] Pierre Comon. Independent component analysis, 1992.
- [16] Wilhelmus HA Schilders, Henk A Van der Vorst, and Joost Rommes. *Model order reduction: theory, research aspects and applications*, volume 13. Springer, 2008.
- [17] Mehryar Mohri, Afshin Rostamizadeh, and Ameet Talwalkar. *Foundations of machine learning*. MIT press, 2018.
- [18] Michael I Jordan and Tom M Mitchell. Machine learning: Trends, perspectives, and prospects. *Science*, 349(6245):255–260, 2015.
- [19] Yue Liu, Tianlu Zhao, Wangwei Ju, and Siqi Shi. Materials discovery and design using machine learning. *Journal of Materiomics*, 3(3):159–177, 2017.
- [20] Weiyu Wang and Keng Siau. Artificial intelligence, machine learning, automation, robotics, future of work and future of humanity: A review and research agenda. *Journal of Database Management (JDM)*, 30(1):61–79, 2019.
- [21] Keith Worden and Graeme Manson. The application of machine learning to structural health monitoring. *Philosophical Transactions of the Royal Society A: Mathematical, Physical and Engineering Sciences*, 365(1851):515–537, 2007.
- [22] Thorsten Wuest, Daniel Weimer, Christopher Irgens, and Klaus-Dieter Thoben. Machine learning in manufacturing: advantages, challenges, and applications. *Production & Manufacturing Research*, 4(1):23–45, 2016.
- [23] Warren S Sarle. Neural networks and statistical models. 1994.
- [24] Kevin Gurney. *An introduction to neural networks*. CRC press, 2018.
- [25] Maziar Raissi, Paris Perdikaris, and George E Karniadakis. Physics-informed neural networks: A deep learning framework for solving forward and inverse problems involving nonlinear partial differential equations. *Journal of Computational Physics*, 378:686–707, 2019.
- [26] Adrian Silvescu. Fourier neural networks. In *IJCNN’99. International Joint Conference on Neural Networks. Proceedings (Cat. No. 99CH36339)*, volume 1, pages 488–491. IEEE, 1999.
- [27] Lu Lu, Pengzhan Jin, Guofei Pang, Zhongqiang Zhang, and George Em Karniadakis. Learning nonlinear operators via deeponet based on the universal approximation theorem of operators. *Nature Machine Intelligence*, 3(3):218–229, 2021.
- [28] Tianping Chen and Hong Chen. Universal approximation to nonlinear operators by neural networks with arbitrary activation functions and its application to dynamical systems. *IEEE Transactions on Neural Networks*, 6(4):911–917, 1995.
- [29] Ludwig Arnold. Stochastic differential equations. *New York*, 1974.
- [30] Yongqin Xian, Christoph H Lampert, Bernt Schiele, and Zeynep Akata. Zero-shot learning—a comprehensive evaluation of the good, the bad and the ugly. *IEEE transactions on pattern analysis and machine intelligence*, 41(9):2251–2265, 2018.
- [31] Steven Atkinson and Nicholas Zabaras. Structured bayesian gaussian process latent variable model: Applications to data-driven dimensionality reduction and high-dimensional inversion. *Journal of Computational Physics*, 383:166–195, 2019.
- [32] Souvik Chakraborty and Rajib Chowdhury. Graph-theoretic-approach-assisted gaussian process for nonlinear stochastic dynamic analysis under generalized loading. *Journal of Engineering Mechanics*, 145(12):04019105, 2019.
- [33] Souvik Chakraborty. Transfer learning based multi-fidelity physics informed deep neural network. *Journal of Computational Physics*, 426:109942, 2021.

- [34] Souvik Chakraborty and Rajib Chowdhury. Moment independent sensitivity analysis: H-pcfe-based approach. *Journal of Computing in Civil Engineering*, 31(1):06016001, 2017.
- [35] Souvik Chakraborty and Rajib Chowdhury. Polynomial correlated function expansion. In *Modeling and simulation techniques in structural engineering*, pages 348–373. IGI global, 2017.
- [36] Ove Ditlevsen and Henrik O Madsen. *Structural reliability methods*, volume 178. Wiley New York, 1996.
- [37] Loren D Lutes and Shahram Sarkani. Reliability analysis of systems subject to first-passage failure. 2009.
- [38] Martín Abadi, Paul Barham, Jianmin Chen, Zhifeng Chen, Andy Davis, Jeffrey Dean, Matthieu Devin, Sanjay Ghemawat, Geoffrey Irving, Michael Isard, et al. Tensorflow: A system for large-scale machine learning. In *12th {USENIX} symposium on operating systems design and implementation ({OSDI} 16)*, pages 265–283, 2016.
- [39] Yi-Kwei Wen. Method for random vibration of hysteretic systems. *Journal of the engineering mechanics division*, 102(2):249–263, 1976.
- [40] Hong-guang Li and Guang Meng. Nonlinear dynamics of a sdf oscillator with bouc-wen hysteresis. *Chaos, Solitons & Fractals*, 34(2):337–343, 2007.
- [41] Abien Fred Agarap. Deep learning using rectified linear units (relu). *arXiv preprint arXiv:1803.08375*, 2018.
- [42] Xavier Glorot and Yoshua Bengio. Understanding the difficulty of training deep feedforward neural networks. In *Proceedings of the thirteenth international conference on artificial intelligence and statistics*, pages 249–256. JMLR Workshop and Conference Proceedings, 2010.
- [43] Sina Shirali. Principal component and independent component regression for predicting the responses of nonlinear base isolated structures. Master’s thesis, University of Waterloo, 2009.
- [44] Jann N Yang, Anil K Agrawal, Bijan Samali, and Jong-Cheng Wu. Benchmark problem for response control of wind-excited tall buildings. *Journal of engineering mechanics*, 130(4):437–446, 2004.
- [45] Rajdip Nayek, Souvik Chakraborty, and Sriram Narasimhan. A gaussian process latent force model for joint input-state estimation in linear structural systems. *Mechanical Systems and Signal Processing*, 128:497–530, 2019.
- [46] tf.keras.layers.normalization, 2021. Accessed: 10 Jan 2022, 0040 Hrs.